

Mark E. Baird

## Numerical approximations of the mean absorption cross-section of a variety of randomly oriented microalgal shapes

Received: 12 March 2002 / Revised version: 14 January 2003 /  
Published online: 12 June 2003 – © Springer-Verlag 2003

**Abstract.** The size, shape, and absorption coefficient of a microalgal cell determines, to a first order approximation, the rate at which light is absorbed by the cell. The rate of absorption determines the maximum amount of energy available for photosynthesis, and can be used to calculate the attenuation of light through the water column, including the effect of packaging pigments within discrete particles. In this paper, numerical approximations are made of the mean absorption cross-section of randomly oriented cells,  $\overline{aA}$ . The shapes investigated are spheroids, rectangular prisms with a square base, cylinders, cones and double cones with aspect ratios of 0.25, 0.5, 1, 2, and 4. The results of the numerical simulations are fitted to a modified sigmoid curve, and take advantage of three analytical solutions. The results are presented in a non-dimensionalised format and are independent of size. A simple approximation using a rectangular hyperbolic curve is also given, and an approach for obtaining the upper and lower bounds of  $\overline{aA}$  for more complex shapes is outlined.

### 1. Introduction

Microalgae come in a wide range of shapes and sizes [4]. The effect of cell size and shape on light absorption can be approximated using an absorption cross-section,  $aA$  [7]. For a cell in an unidirectional incident light field,  $I$ , the average rate of light absorbed by one cell,  $P$ , is given by:

$$P = \overline{aA}I \quad (1)$$

where the bar signifies the mean absorption cross-section over a random orientation. A random orientation is investigated because microalgal cells in a turbulent fluid are unable to orient themselves. The contribution of  $n$  cells per unit volume to the attenuation coefficient of water per unit length is  $n\overline{aA}$ . The absorption cross-section of cells over a random orientation is useful for calculations of light attenuation in natural water bodies such as rivers, estuaries and the open ocean.

The rate at which a cell absorbs light affects the attenuation of light within the water column in two ways. Firstly, the packaging of pigments within cells, as opposed to an even distribution of dissolved pigment, reduces the rate of light

---

M.E. Baird: School of Mathematics, University of New South Wales, Sydney 2052, Australia. e-mail: mbaird@maths.unsw.edu.au

*Key words or phrases:* Shape – Plankton – Absorption cross-section – Rectangular prism – Cone – Cylinder – Random orientation

attenuation. The larger the cells and the more concentrated the pigments are within the cells, the greater the increase in light penetration. Secondly, since microalgae have wavelength-dependent absorbance rates, the shape of the cells also alters the colour of light as it is transmitted through the water column [6]. The inclusion of these effects in models of light attenuation is important when correlating the rate of light attenuation with chlorophyll or microalgal biomass [7].

For the sake of explanation,  $\overline{aA}$  can be split into two separate variables, where  $A(\psi, \theta)$  is the cross-sectional area perpendicular to the light, or the projected area, and  $a(l, t, \psi, \theta)$  is the fraction of light absorbed for a particular pencil of light through the shape (Figure 1). The projected area,  $A(\psi, \theta)$ , is a function of the orientation of the shape, as specified by two orthogonal angles,  $\psi$  and  $\theta$ . The fraction of light absorbed,  $a$ , is a function of the orientation of the shape, and the particular pencil of light, which is specified by coordinates  $l$  and  $t$ , and is given by:

$$a(l, t, \psi, \theta) = 1 - e^{\gamma C d(l, t, \psi, \theta)} \quad (2)$$

where  $\gamma C$  is the absorption coefficient, or absorbance per unit length of the light as it travels through the shape,  $d(l, t, \psi, \theta)$  is the distance the pencil takes through the shape,  $\gamma$  is the pigment specific absorption coefficient, and  $C$  is the concentration of the pigment within the cell. Both  $a$  and  $A$  vary with shape and orientation, and, in general,  $\overline{a}$  multiplied by  $\overline{A}$  is not equal to  $\overline{aA}$ . Therefore the results in this paper are presented as  $\overline{aA}$ , the mean absorption cross-section over a random orientation.

Analytical solutions for  $\overline{aA}$  are available for a sphere, prolate and oblate spheroids, and an infinitely long cylinder [6], but are difficult to obtain for geometries in which the whole surface of the shape is not defined by one co-ordinate. For example, the surface of a sphere can be defined in spherical co-ordinates by setting the radial co-ordinate to a constant value. In contrast, the surface of a cube is defined by six different planes, which cannot be simply represented by one co-ordinate system. Furthermore, while an analytical solution is known for spheroids, it involves a computationally expensive triple integral, and has not been utilised as much as might be expected.

In this paper, numerical approximations of the randomly oriented absorption cross-section of spheroids, rectangular prisms with a square base, cylinders, cones and double cones with aspect ratios,  $p$ , of 0.25, 0.5, 1, 2, and 4 are determined. The shapes are all symmetrical about the horizontal plane and the aspect ratio is defined as the height of the shape divided by the width or diameter in the symmetrical plane (Figure 1).

## 2. Methods

The mean absorption cross-section is calculated based on the assumption that the wavelength of light passing through the shape is small relative to pathlength through the shape, and that the attenuating pigments are evenly distributed throughout the shape. For the numerical calculations, the shape is rotated at an angle  $\psi$  around the Z-axis, while light incident to the shape is rotated at an angle  $\theta$  around the X-axis (Figure 1). A random orientation is modelled by running a large number of simulations,  $S$ , with the angles  $\theta$  and  $\psi$  chosen randomly for each simulation [8].  $\psi$  is

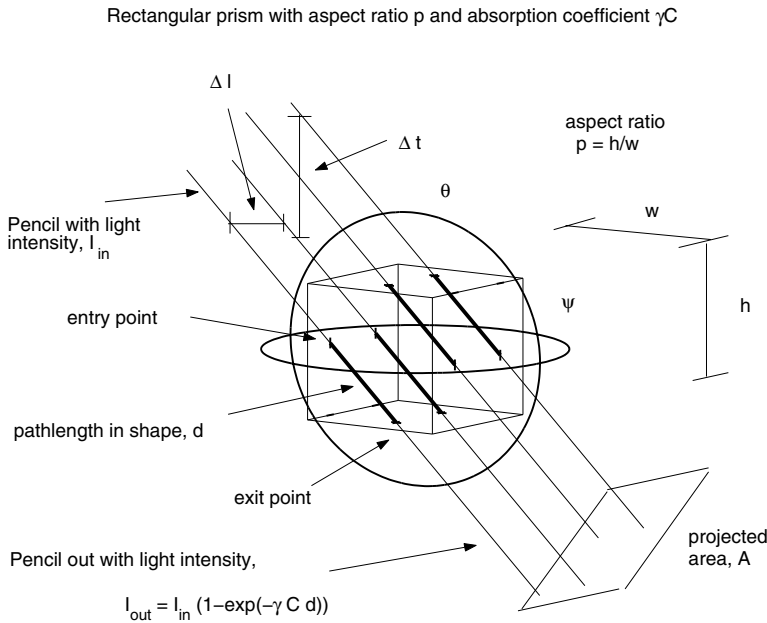


**Fig. 1.** Schematic of the numerical simulations of the absorption cross-section of a rectangular prism of aspect ratio  $p = h/w$ . Four pencils of light travel a distance  $d(l, t)$  through the shape at an angle  $\theta$  from the horizontal, while the shape is rotated in horizontal plane by an angle  $\psi$ . The light pencils are separated by a distance  $\Delta l$  and  $\Delta t$ . The shape casts a shadow, or projected area, of  $A$ .

given a uniform random distribution, while  $\theta$  is based on the *arccosine* of a uniform distribution. The skewed distribution of  $\theta$  accounts for the greater likelihood of an orientation with low values of  $\theta$ , and is analogous to the greater distance between lines of longitude on the Earth at low latitudes [2].

Light is modelled as a 2-dimensional array of light pencils. The array has co-ordinates  $t$  and  $l$ , with a total of  $n_t$  and  $n_l$  pencils, each separated by a distance  $\Delta t$  and  $\Delta l$  in the  $t$  and  $l$  directions. The array extends beyond the edges of the shape in all directions. Each pencil of light is represented in parametric form, and solved simultaneously with an equation representing each surface or plane of the shape. The solution is an exact value (within software precision) for the entry and exit co-ordinates of the pencil. The straight line distance between the entry and exit co-ordinates is calculated for simulation  $s$  and pencil  $(l, t)$ , as  $d(l, t, s)$ . From the numerical simulations,  $\overline{aA}$  is approximated as the mean  $aA$  for  $S$  random orientations:

$$\overline{aA}_{NS} = \frac{1}{S} \sum_{s=0}^S \sum_{l=0}^{n_l} \sum_{t=0}^{n_t} \left( 1 - e^{-\gamma C d(l,t,s)} \right) \Delta l \Delta t \quad (3)$$

To ensure the light pencils completely surround the shape, a test for  $d(l, t, s) = 0$  for all values of  $t = 0, l = 0, t = n_t$  and  $l = n_l$  can be undertaken. The results

in this paper are based on a  $500 \times 500$  array of light pencils and 200 random orientations.

The results of simulations for a particular shape and range of absorbances are used to determine the parameter values and undertake an error analysis for two curves, a rectangular hyperbolic (RH) curve and a modified sigmoid (MS) curve, that give  $\overline{aA}$  as a function of  $\gamma C$ . In both relationships,  $\gamma C$  is multiplied by  $r_{ESR}$  to give the non-dimensional quantity,  $\gamma Cr_{ESR}$ , where  $r_{ESR}$  is the radius of a sphere with an equivalent volume. The use of  $\gamma Cr_{ESR}$  facilitates the comparison of results between different sizes, shapes and aspect ratios. Most importantly, the results are independent of the size of the cell. Values of  $\overline{aA}_{NS}$  at  $\gamma Cr_{ESR} = 0, 0.2, 0.4, \dots, 4.6, 4.8, 5, 10, 15, 20$  were obtained for each simulation.

The results of the numerical simulations are analysed in the context of three useful analytical solutions:

1. The initial slope of the curve of  $\overline{aA}$  against  $\gamma Cr_{ESR}$  for all shapes and orientations is given by:

$$\lim_{\gamma C \rightarrow 0} \frac{d \overline{aA}}{d \gamma Cr_{ESR}} = \frac{4}{3} \pi r_{ESR}^2 \tag{4}$$

This result can be shown for a rectangular prism  $4\pi r_{ESR}/3 \times r_{ESR} \times r_{ESR}$ , with light pencils parallel to one of the  $r_{ESR}$  dimensions. For this shape,  $aA = 4\pi r_{ESR}^2 (1 - e^{-\gamma Cr_{ESR}}) / 3$  where  $A = 4\pi r_{ESR}^2 / 3$  and  $a$  is obtained from Eq. 2. The differential of  $aA$  with respect to  $\gamma Cr_{ESR}$  as  $\gamma C$  approaches zero is  $4\pi r_{ESR}^2 / 3$ . At low  $\gamma C$ ,  $\overline{aA}$  is equal for all shapes of equal volume at all orientations [6], so Eq. 4 is true for all orientations of any shape.

2. For a randomly oriented convex shape the mean projected area,  $\overline{A}$ , is given by the total surface area divided by 4:

$$\overline{A} = \frac{\text{Surface Area}}{4} \tag{5}$$

This result comes from the work of Cauchy [3] presented in 1832 [8].

3. The analytical solution of  $\overline{aA}$  for a sphere of radius  $r$  is given by [5]:

$$\overline{aA}_{sphere} = \pi r^2 \left( 1 - \frac{2(1 - (1 + 2\gamma Cr) e^{-2\gamma Cr})}{(2\gamma Cr)^2} \right) \tag{6}$$

*Curve fitting.* The RH curve of  $\overline{aA}$  as a function of  $\gamma Cr_{ESR}$  is given by:

$$\overline{aA}_{RH} = \frac{\overline{A} \gamma Cr_{ESR}}{\frac{3\overline{A}}{4\pi r_{ESR}^2} + \gamma Cr_{ESR}} \tag{7}$$

In fact, the RH curve does not directly use the results of the numerical simulations. Simply, it fits the RH curve to the analytical endpoints (Eqs. 4 & 5). Since no parameters require fitting to numerical simulations, the RH curve can be used for any convex shape for which the surface area is known. The results of the numerical simulations are used to determine the accuracy of the RH curve for non-spheroidal shapes.

The MS curve takes advantage of all three analytical solutions. The results of the numerical simulations are used to determine the fitted parameter,  $k$ , and to estimate the maximum error in fitting the results of the numerical simulations to the MS curve. The MS curve of  $\overline{aA}$  as a function of  $\gamma C$  is given by:

$$\overline{aA}_{MS} = \overline{aA}_{sphere} + \frac{(\overline{A} - \pi r_{ESR}^2) (\gamma C r_{ESR})^2}{k^2 + (\gamma C r_{ESR})^2} \tag{8}$$

Eq. 8 is based on the addition of the analytical solution for a sphere of the same volume,  $\overline{aA}_{sphere}$  (Eq. 6), and a sigmoid term. A sphere has the lowest  $\overline{aA}$  for any shape of the same volume. The sigmoid term is approximating the effect of the non-spherical geometry of the shape. By building the solution on that of sphere, Eq. 8 is taking advantage of the form of the analytical solution of the sphere. The sigmoid term has a zero value at  $\gamma C = 0$ , which gives the shape the same initial slope of  $\overline{aA}$  against  $\gamma C$ , in agreement with Eq. 4, and a maximum of the difference in mean projected area of the shape and a sphere of equivalent volume,  $\overline{A} - \pi r_{ESR}^2$ , so agreeing with Eq. 5.

Algal cells generally have a value of  $\gamma C r_{ESR}$  of less than 5. The parameter  $k$  is determined by the value which minimises the difference between the results of the numerical simulations and the MS curve in the region  $\gamma C r_{ESR} \leq 5$ . Note that even though the fit for  $k$  is undertaken for  $\gamma C r_{ESR} \leq 5$ , the value of  $\overline{aA}$  at high  $\gamma C r_{ESR}$  is still constrained by the analytically determined value for  $\overline{A}$ .

### 3. Error analysis

An initial assessment of the errors in the numerical approximation of  $\overline{aA}$  can be made by undertaking numerical calculations of volume and mean projected area. A measure of the accuracy of the simulations in determining the average pathlength of a light pencil through the shape, a critical component of the calculation of  $\overline{aA}$ , can be determined by numerically determining the volume of the shape. Using the same techniques as for the calculation of  $\overline{aA}$ , the volume is calculated as the sum for each pencil of the multiple of the pathlength of the pencil through the shape,  $d$ , and the area,  $\Delta t \Delta l$ , the pencil represents. The numerical approximation of the volume of the shape for simulation  $s$  is given by:

$$V_{NS}(s) = \sum_{l=1}^{n_l} \sum_{t=1}^{n_t} (d(l, t, s) \Delta t \Delta l), \tag{9}$$

The error in the numerical approximation of volume is given by:

$$E_V^{NS}(s) = \frac{100 |V_{NS}(s) - V|}{V} \tag{10}$$

where  $V$  is the analytical solution for the volume of the shape. The error in calculating the distance  $d$  is based on software precision (for the MATLAB software package used software precision is  $2^{-52}$ ). A limiting factor in the numerical estimation of  $V$  (and hence in  $\overline{aA}$ ) is the number of pencils. The more pencils used, the better the edges of the shape are resolved. For all cases presented in this paper, an array

of  $500 \times 500$  pencils of light was used and the resulting error,  $E_V^{NS}$ , for all shapes and orientations was less than 0.5%.

At a high absorbance  $\overline{aA}$  should converge on the analytically calculated mean projected area for a randomly oriented shape,  $\overline{A}$ , as given in Eq. 5. The error introduced in the numerical integration of  $aA$  over a random orientation,  $E_{\overline{A}}$ , is measured as the percent difference between the numerical approximation of  $\overline{aA}$  at a very high absorbance,  $\overline{aA}_{\gamma C \rightarrow \infty}$ , and the analytical solution,  $\overline{A}$ :

$$E_{\overline{A}} = 100 \frac{|\overline{aA}_{\gamma C \rightarrow \infty} - \overline{A}|}{\overline{A}} \quad (11)$$

For spheroids, an analytical solution of  $\overline{aA}$  as a function of  $\gamma C$ ,  $\overline{aA}_{AS}$ , is available [6]. Therefore, a direct determination of the percent error in the numerical approximation of  $\overline{aA}$ ,  $\overline{aA}_{NS}$ , at each of the values of  $\gamma C_{RESR}$ , can be determined. The maximum error in  $aA_{NS}$  is given by:

$$E_{\overline{aA}} = 100 \max \left( \frac{|\overline{aA}_{AS} - \overline{aA}_{NS}|}{\overline{aA}_{AS}} \right) \quad (12)$$

where the maximum function applies to the values of bracketed expression at values of  $\gamma C_{RESR} = 0, 0.2, \dots, 4.8, 5, 10, 15, 20$  and noting that the percent error is always positive. Similar use of the maximum function over the range of  $\gamma C_{RESR}$  values is made in Eqs. 13, 14, 15 and 16 below. Note that the analytical solution is a triple integral, and must itself be evaluate using numerical techniques. The MATLAB adaptive Lobatto quadrature function with a tolerance  $10^{-6}$  for each integration was used.  $E_{\overline{aA}}$  cannot be determined for non-spheroidal shapes, since there are no analytical solutions for  $\overline{aA}$ . Nonetheless, the results of  $E_{\overline{aA}}$  for spheroidal shapes of a range of aspect ratios gives an indication of the corresponding values for non-spheroidal shapes.

The numerical simulations are fitted to RH and MS curves. For spheroids, the error in the curve approximating  $\overline{aA}$  as a function of  $\gamma C_{RESR}$  is determined as the maximum percent difference between the the curve fits and the analytical solutions:

$$E_{MS}^{AS} = 100 \max \left( \frac{|\overline{aA}_{AS} - \overline{aA}_{MS}|}{\overline{aA}_{AS}} \right) \quad (13)$$

$$E_{RH}^{AS} = 100 \max \left( \frac{|\overline{aA}_{AS} - \overline{aA}_{RH}|}{\overline{aA}_{AS}} \right) \quad (14)$$

where the superscript  $AS$  indicates that the analytical solution for  $\overline{aA}$  has been used, and  $\overline{aA}_{MS}$  and  $\overline{aA}_{RH}$  are the values of  $\overline{aA}$  obtained using Eqs. 8 & 7 respectively.

For non-spheroids, where no analytical solutions are available, the maximum error is determined as the maximum percent difference between the results of the numerical simulations and the curve themselves:

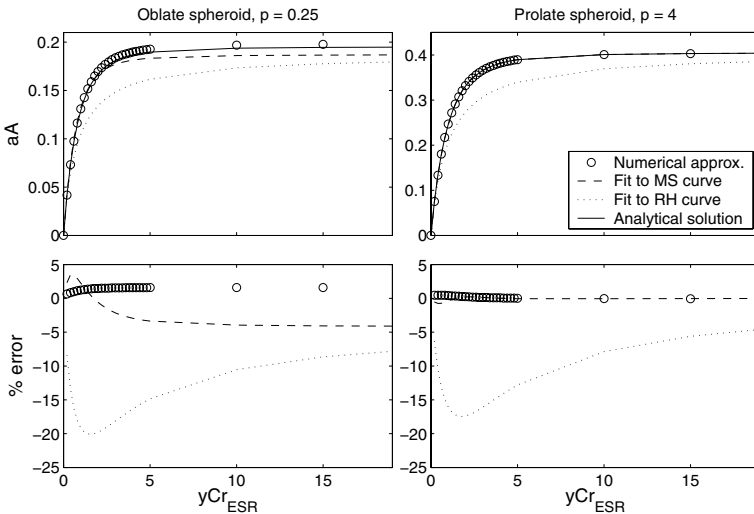
$$E_{MS}^{NS} = 100 \max \left( \frac{|\overline{aA}_{NS} - \overline{aA}_{MS}|}{\overline{aA}_{NS}} \right) \quad (15)$$

$$E_{RH}^{NS} = 100 \max \left( \frac{|\overline{aA_{NS}} - \overline{aA_{RH}}|}{\overline{aA_{NS}}} \right) \tag{16}$$

where the superscript *NS* indicates that the numerical simulations have been used to determine the error.

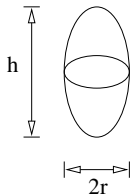
#### 4. Results

*Spheroids.* The analytical solutions and numerical approximations of  $\overline{aA}$  for an oblate ( $p = 0.25$ ) and prolate ( $p = 4$ ) spheroid as a function of  $\gamma Cr_{ESR}$  are graphed in Figure 2. Figure 2 also gives the percentage errors between the analytical solution and the numerical approximations. The maximum error between the analytical solution and the numerical simulations for the prolate spheroid (at  $p = 4$ ),  $E_{\overline{aA}}$ , is 0.47% (Table 1). Only a small portion of this error,  $E_{\overline{A}} = 0.07\%$ , can be attributed to the integration over a random orientation. The maximum error in fitting the numerical approximations to the MS curve,  $E_{MS}^{AS}$ , is 0.74%, although a much greater maximum error occurred when fitting to a RH curve,  $E_{RH}^{AS} = 17.5\%$ . The  $\overline{aA}$  for an oblate spheroid was less well approximated by the numerical approximations. In particular, the error in integrating over a random orientation is significantly greater than for the prolate spheroid. Nonetheless,  $E_{\overline{aA}}$ ,  $E_{\overline{A}}$  and  $E_{MS}^{AS}$  were all 6% or less for aspect ratios of 0.25 and 0.5. In general, the errors in the numerical simulations, and in the MS curve fit are small, and give confidence in the curve fits for non-spheroidal shapes, in which no analytical solution is available for a direct measure of errors.



**Fig. 2.** Analytical, numerical and curve fit results for an oblate and prolate spheroid of aspect ratios 0.25 and 4 respectively. The fit to the MS curve for the prolate spheroid is obscured by the analytical result. Note the magnitude of  $\overline{aA}$  is different from Fig. 3. because spheroids of smaller volume were used.

**Table 1.** Data from the numerical simulations of the randomly oriented absorption cross-section,  $\bar{a}\bar{A}$ , of spheroidal microalgal shapes at a range of aspect ratios. The spheroid is defined on the left.  $\bar{A}$  is the analytically determined projected area over a random orientation as given by Eq. 5.  $k$  is the fitted parameter for the MS curve (Eq. 8). The right four columns give result of the error analysis (for definitions of  $E_{\bar{A}}$ ,  $E_{\bar{a}\bar{A}}$ ,  $E_{MS}^{AS}$  and  $E_{RH}^{AS}$  see Error Analysis section).

shape	aspect ratio $h/2r$	$k$	Errors%			
			simulations		curve fit	
			$E_{\bar{A}}$	$E_{\bar{a}\bar{A}}$	$E_{MS}^{AS}$	$E_{RH}^{AS}$
 spheroid	0.25	0.5	6.0	1.59	4.11	20.1
	0.5	1.8	0.54	0.54	0.23	17.8
	2	1.6	0.02	0.39	0.14	18.3
	4	1.7	0.07	0.47	0.74	17.5
$h/2r < 1$	$\bar{A} = \frac{\pi hr}{4} \left[ \frac{2r}{h} + \frac{h/2}{\sqrt{r^2 - h^2/4}} \ln \left( \frac{r + \sqrt{r^2 - h^2/4}}{h/2} \right) \right]$					
$h/2r > 1$	$\bar{A} = \frac{\pi r}{4} \left( 2r + \frac{h^2}{\sqrt{h^2 - 4r^2}} \sin^{-1} \frac{\sqrt{h^2 - 4r^2}}{h} \right)$					

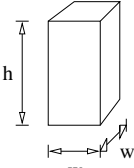
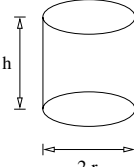
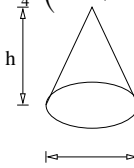
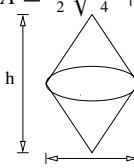
*Prisms, cylinders and cones.* Table 2 gives the results for  $k$ ,  $E_{\bar{A}}$ ,  $E_{MS}^{NS}$  and  $E_{RH}^{NS}$  for non-spherical shapes. As noted above, the results for non-spherical shapes have no analytical solutions to be compared to (other than for  $\bar{A}$ ) so  $E_{MS}$  and  $E_{RH}$  are based on  $\bar{a}A_{NS}$ . The MS curve appears to well represent the numerical simulations, with only the flattest cone ( $p = 0.25$ ) having a maximum error greater than those for the spheroids.

General comments on the effectiveness of light capture per unit volume of different shapes are now possible. Figure 3 displays the MS curve fits for cells of equal volume but varying shape and aspect ratio. The results illustrate that: (1) shape dependent properties of light capture only become important for  $\gamma Cr_{ESR} > 1$ ; (2) for all shapes and absorbances, a shape with an aspect ratio of 1 is the least effective at capturing light; (3) that decreasing the aspect ratio (flattening the shape) is more effective at increasing light capturing than increasing the aspect ratio (elongating the shape); and (4) cones had the most pronounced increase in absorption cross-section with decreasing aspect ratio.

The error analysis showed that the numerical simulations and the curve fits were generally best at an aspect ratio of 1, worsening more as the shape becomes flatter



**Table 2.** Data from the numerical simulations of the randomly oriented absorption cross-section,  $a\bar{A}$ , of non-spheroidal microalgal shapes at a range of aspect ratios. The shape is defined on the left, with  $\bar{A}$ , the analytically-determined projected area over a random orientation as given by Eq. 5.  $k$  is the fitted parameter for the MS curve (Eq. 8). The right three columns give result of the error analysis (for definitions of  $E_{\bar{A}}$ ,  $E_{MS}^{NS}$  and  $E_{RH}^{NS}$  see Error Analysis section).

shape	aspect ratio $h/2r, h/w$	$k$	Errors%		
			simulations $E_{\bar{A}}$	curve fit $E_{MS}^{NS}$ $E_{RH}^{NS}$	
$\bar{A} = (2w + 4h) w/4$					
 rectangular prism	0.25	2.0	3.46	1.75	14.8
	0.5	3.0	0.29	2.52	12.5
	1	3.3	1.90	1.31	12.4
	2	3.4	0.22	2.72	12.0
	4	2.4	0.77	3.24	12.8
$\bar{A} = \pi r (r + h) /2$					
 short cylinder	0.25	2.0	2.01	1.50	14.7
	0.5	2.5	2.39	1.23	14.8
	1	3.1	1.51	0.82	15.0
	2	2.1	1.45	1.23	15.9
	4	1.7	0.34	1.41	16.9
$\bar{A} = \frac{\pi r}{4} (r + \sqrt{h^2 + r^2})$					
 cone	0.25	3.8	2.23	7.61	2.17
	0.5	2.9	2.12	2.80	9.37
	1	3.1	0.53	1.84	12.3
	2	2.4	0.58	1.57	14.0
	4	2.0	0.71	1.89	14.7
$\bar{A} = \frac{\pi r}{2} \sqrt{\frac{h^2}{4} + r^2}$					
 double cone	0.25	2.9	4.08	4.87	7.14
	0.5	2.8	1.94	2.47	11.2
	1	3.5	0.08	1.08	15.6
	2	2.5	0.25	0.84	16.5
	4	2.0	0.22	1.31	15.5

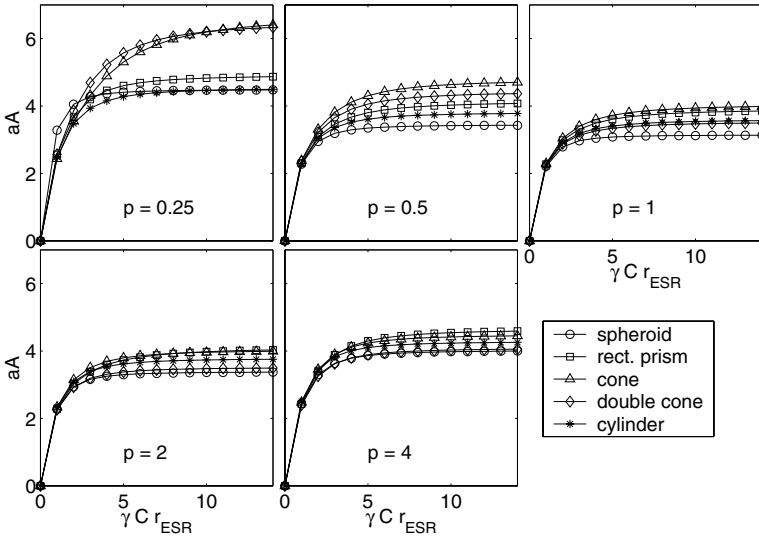


**Fig. 3.** The MS curve fit of the mean absorption cross-section,  $\overline{aA}_{MS}$ , of a spheroid, rectangular prism with a square based, cone, double cone and cylinder of volume  $4\pi/3$  (i.e.  $r_{ESR} = 1$ ) at aspect ratios,  $p$ , of 0.25, 0.5, 1, 2, 4 against the non-dimensional absorbance,  $\gamma C r_{ESR}$ .

when compared to becoming more elongated. This trend can be largely attributed to the sensitivity of a flat object's projected area to its orientation. It also appears that the MS curve does not capture the underlying relationship between  $\overline{aA}$  and  $\gamma C$  as well for a flat object as for an elongated shape. Surprisingly, a cone of  $p = 0.25$  is better fitted by the RH curve than the MS curve.

## 5. Discussion

The results of numerical simulations on spheroids, rectangular prisms with a square based, cones and cylinders of aspect ratios 0.25, 0.5, 1, 2, 4 were fitted to two curves, a MS curve and a RH curve. The error in the RH curve fit was always less than 21%, and typical had values between 10 and 20%. The RH curve provides a reasonable fit to any convex shapes for which the surface area is known. The MS curve provides a much more accurate fit, with a maximum error always less than 8% and often around 1%.

The results from this study are intended to fill a gap in the analytical solutions for non-spheroidal shapes. When using these results, the source of errors in the numerical approximations should be kept in mind. In particular, the random orientation is modelled using a set of 200 random numbers. A different set of random numbers is likely to produce slightly different results. Furthermore, the parameter  $k$  has been obtained to minimise the maximum percent difference between the numerical simulations and MS curve for  $\gamma C r_{ESR} \leq 5$ . Another curve fitting criteria may produce slightly different values of  $k$ . Nonetheless, the approach of

undertaking numerical simulations and fitting these results to curves constrained by analytical solutions has produced relatively small errors and fills a gap in the available analytical solutions.

This study was motivated by a desire to obtain approximations of  $\overline{aA}$  for a range of shapes more representative of known microalgal cells than is provided by spheroids and infinitely long cylinders alone. Hillebrand *et al.* [4] has categorized 850+ microalgal genera into 20 geometric models, with a small number of exceptions and composite shapes (i.e. two ellipsoids). Of the 870 individual listings, the most common shapes in decreasing order are prolate spheroids (157), cylinders (151), spheres (141), elliptical prisms (112), ellipsoids (86), rectangular boxes (42), double cones (30), and cones with a half sphere (24). Excluding the list of exceptions, only 29 genera had shapes that were not defined by one of the Hillebrand's standard 20 geometric models.

For shapes that do not have known analytical solutions or numerical approximations for  $\overline{aA}$ , upper and lower bounds of the value  $\overline{aA}$  may take can be determined. The upper bound of  $\overline{aA}$  of an unknown shape is given by the  $\overline{aA}$  for a known shape that surrounds the unknown shape. The lower bound is given by the  $\overline{aA}$  of any known shape that fits within the unknown shape. For example, a cylinder of radius  $r$  and height  $h$ , with two half spheres on each end has an upper limit of a cylinder of radius  $r$ , and height  $h + 2r$ , and a lower limit of a spheroid of radius  $r$  and aspect ratio of  $h + 2r/2r$ . Similarly, the upper and lower bounds of other shapes defined in Hillebrand *et al.* [4] can be determined: an ellipsoid by two spheroids; a cylinder + 2 cones by a cylinder and a prolate spheroid; and a cone + half sphere by a sphere and a double cone. A rectangular box, a prism on an elliptic base, a prism on a parallelogram-base, a half-elliptic prism and a prism on a triangle-base have upper and lower bounds of two rectangular prisms with square bases. A pyramid can be approximated by two cones. The difference between the upper and lower bounds of these shapes will depend on the ratio of the different dimensions defining the shape, but in general are not large.

Of the 20 geometrical shapes defined in Hillebrand *et al.* [4], only the sickle-shaped prism (4 genera), the monoraphidioid (included as an exception only) and the elliptic prism with a transapical constriction (no genera listed) are concave in nature. In order to take advantage of Cauchy's theorem (Eq. 5), the above analysis has been restricted to convex shapes. In general, convex shapes provide poor upper and lower bounds for concave shapes.

Some complex shapes such as the cymbelloid (11 genera listed), the elliptic prism with transapical inflations (1) and the gomphonemoid (12) are convex, but do not naturally fit the shapes given in this paper. A further 29 genera are either a combination of shapes, or are a truncated shape, and are not necessarily bounded well by numerical solutions in this paper. Nonetheless, the great majority of the microalgal genera listed by Hillebrand *et al.* [4] have the same shape or are well bounded by shapes for which numerical approximations are given in this paper.

In addition to being useful for modelling light attenuation through the water column (as mentioned in the Introduction), the presented results can be used for modelling light-limited microalgal growth. Under low light conditions, a photosynthetic cell is most efficient at using light that is absorbed. The initial slope of the

growth versus irradiance curve,  $\alpha$ , is proportional to  $\overline{aA}$  [1]. The parameter  $\alpha$  can be approximated as  $\alpha = m_I \overline{aA} I$  where  $m_I$  is 8-10 times the carbon content of the cell in moles, and  $I$  is specified as moles of photons per metre squared [1]. A common alternative formulation for light-limited growth involves using Monod growth curves with fitted half-saturation constants. The use of a geometrically-determined  $\overline{aA}$  instead provides a physical bases for obtaining parameter values.

The numerical approximations presented in this paper may also be useful in the automated identification of microalgae. Recent work has shown that the distribution of the projected area of randomly oriented opaque particles can be used to identify the three dimensional shape that produces the shadow [8]. It is also conceivable that the results presented here may be useful for automated identification of algal genus. Flow cytometry techniques use the alterations in a light field to identify algal sizes. An improved consideration of the effects of microalgal shape on light penetration, combined with a categorisation of algal genera into shapes such as undertaken by Hillebrand *et al.* [4], may improve the capabilities of automated identification techniques.

In summary, the results from this study expand our ability and ease of including the effects of microalgal shape on an unidirectional light field, and has applications in modelling of light limit algal growth, light attenuation in natural water bodies, and in the automated identification of microalgal genus.

*Acknowledgements.* This research was funded in part through Australian Research Council grants held by Jason Middleton, and by Iain Suthers and Mark Baird. The author gratefully acknowledges a very constructive anonymous reviewer, and the help of Peter Oke and Jaclyn Brown.

## References

1. Baird, M.E., Emsley, S.M., McGlade, J.M.: Modelling the interacting effects of nutrient uptake, light capture and temperature on phytoplankton growth. *J. Plankton Res.* **23**, 829–840 (2001)
2. Brown, D.J., Vickers, G.T.: The use of projected area distribution functions in particle shape measurement. *Powder Technology* **98**, 250–257 (1998)
3. Cauchy, A.: *Oeuvres Complètes d'Augustin Cauchy*, 1ere Sér. volume II, pp. 167–177. Gauthier-Villars, Paris, 1908
4. Hillebrand, H., Durselen, C., Kirschtel, D., Pollinger, U., Zohary, T.: Biovolume calculation for pelagic and benthic microalgae. *J. Phycol.* **35**, 403–424 (1999)
5. Kirk, J.T.O.: A theoretical analysis of the contribution of algal cells to the attenuation of light within natural waters. II. Spherical cells. *New Phytol.* **75**, 21–36 (1975)
6. Kirk, J.T.O.: A theoretical analysis of the contribution of algal cells to the attenuation of light within natural waters. III. Cylindrical and spheroidal cells. *New Phytol.* **77**, 341–358 (1976)
7. Kirk, J.T.O.: *Light and Photosynthesis in Aquatic Ecosystems*. Cambridge University Press, Cambridge, 2nd edition, 1994
8. Vickers, G.T., Brown, D.J.: The distribution of projected area and perimeter of convex, solid particles. *Proc. R. Soc. Lond. A* **457**, 283–306 (2001)